Thin Solid Films 519 (2011) 5212–5218

Contents lists available at ScienceDirect

Thin Solid Films

journal homepage: www.elsevier.com/locate/tsf

Applications of novel dithienothiophene- and 2,7-carbazole-based conjugated polymers with surface-modified ZnO nanoparticles for organic photovoltaic cells

Hsiao-Ping Fang [a], I-Hung Chiang [a], Chih-Wei Chu [b,c], Chang-Chung Yang [d], Hong-Cheu Lin [a,*]

[a] Department of Materials Science and Engineering, National Chiao Tung University, Hsinchu, Taiwan (ROC)
[b] Department of Photonics, National Chiao Tung University, Hsinchu, Taiwan (ROC)
[c] Research Center for Applied Sciences, Academia Sinica, Taipei, Taiwan (ROC)
[d] Energy and Environmental Laboratories, Industrial Technology Research Institute, Hsinchu, Taiwan (ROC)

ARTICLE INFO

Available online 21 January 2011

Keywords:
Heteroatom-containing polymer
Conjugated polymer
Solar cell
Surface-modified ZnO nanoparticle

ABSTRACT

Two kinds of novel conjugated polymers containing 2,7-carbazole, thiophene, and fused-dithienothiophene rings as backbones bearing acid-protected and benzoic acid pendants (**PC1** and **PC2**, respectively) were utilized for organic solar cell applications. The absorption spectra of these polymers (in both solutions and solid films) showed an absorption range at 300–580 nm. Furthermore, ZnO nanoparticles were synthesized and surface-modified with pyridyl surfactants (**ZnOpy**) to be ca. 3–4 nm. The pyridyl surfactants of **ZnOpy** nanoparticles (as electron acceptors to partially replace expensive electron acceptor PCBM) not only induce supramolecular interactions with benzoic acid pendants of polymer **PC2** via H-bonds, but also enhance the homogeneous dispersions of **ZnOpy** nanoparticles in polymer **PC2**. Thus, the ternary systems of **PC1–PC2**/**ZnOpy**/PCBM in weight ratios of 1:0.05:1 and 1:0.1:1 were investigated in bulk heterojunction polymer solar cells (PSCs). Under the standard illumination of AM 1.5, 100 mW/cm^2, the best power conversion efficiency (PCE) of the PSC cell containing a polymer blend of **PC2**/**ZnOpy**/PCBM = 1:0.05:1 reached PCE = 0.55%, with J_{sc} = 2.11 mA/cm^2, V_{oc} = 0.88 V, and FF = 29.4%.

1. Introduction

The developments of new materials to be used in organic optoelectronic devices such as polymeric solar cells (PSCs) have become dramatically attractive because they represent a green and renewable energy alternative to fossil energy and nuclear power. In particular, the so-called bulk heterojunction (BHJ) concept [1] has been established in thin films of organic solar cell devices utilizing electron-donating conjugated polymers blended with electron-accepting species, such as fullerenes [2], dicyano-based polymers [3,4], or n-type nanoparticles [5]. These hybrid polymer-inorganic solar cells utilize the high electron mobility of the inorganic phase to overcome charge-transport limitations associated with organic materials. The efficient BHJ solar cells made of ZnO nanoparticles and a conjugated polymer have been reported previously [6]. The ZnO nanoparticles were blended with poly[2-methoxy-5-(3′,7′-dimethyloctyloxy)-*p*-phenylenevinylene] (MDMO-PPV) to possess a highest power conversion efficiency (PCE) approaching 1.6% in PSCs [7]. Hybrid solar cells based on CdSe nanoparticles and a PPV-type polymer containing fluorene and thiophene units (PFT) were investigated. The CdSe/PFT devices showed very low photocurrent and fill factor values, which were attributed to the poor charge transport in the trioctylphosphine oxide (TOPO)-capped CdSe nanoparticle phase. Thus, ternary systems based on mixtures of PFT/CdSe and the fullerene derivative [6,6]-phenyl C_{61} butyric acid methyl ester (PCBM) were investigated. It was observed that for the optimized composition of 20 wt.% PFT + 40 wt.% CdSe + 40 wt.% PCBM the devices presented higher photocurrents and efficiencies. The use of inorganic nanoparticles, such as TiO_2, ZnO, $CuInS_2$, PbSe, CdSe, and CdTe, have some advantages, related to the versatility of these materials, which often can be easily synthesized in a great variety of sizes and shapes, according to the desired properties [8].

In parallel, oligo- and poly(2,7-carbazole) [10] derivatives have been successfully used in polymer lightemitting diodes (PLEDs) [11] and organic field-effect transistors (OFETs) [11,12], demonstrating good *p*-type transport properties [9]. Recently, Müllen and co-workers [10] have reported solar cells consisting of poly(*N*-alkyl-2,7-carbazole) with a PCE value of 0.6%. Moreover, in contrast to the fluorene unit the carbazole moiety is fully aromatic, providing a better chemical and environmental stability. Taking all of these results into account, the development of new copolymers based on carbazoles should therefore lead to interesting features for photovoltaic applications. A class of polymers that have to date received little attention as *p*-type materials for use in solar cells is polycarbazoles. Carbazole is a well-known electron-donating unit, and thus poly(2,7-carbazole)s are attractive candidates as *p*-type materials for solar cells [13].

* Corresponding author. Tel.: +886 3 5712121x55305; fax: +886 3 5724727.
E-mail address: linhc@cc.nctu.edu.tw (H.-C. Lin).

0040-6090/$ – see front matter © 2011 Elsevier B.V. All rights reserved.
doi:10.1016/j.tsf.2011.01.162

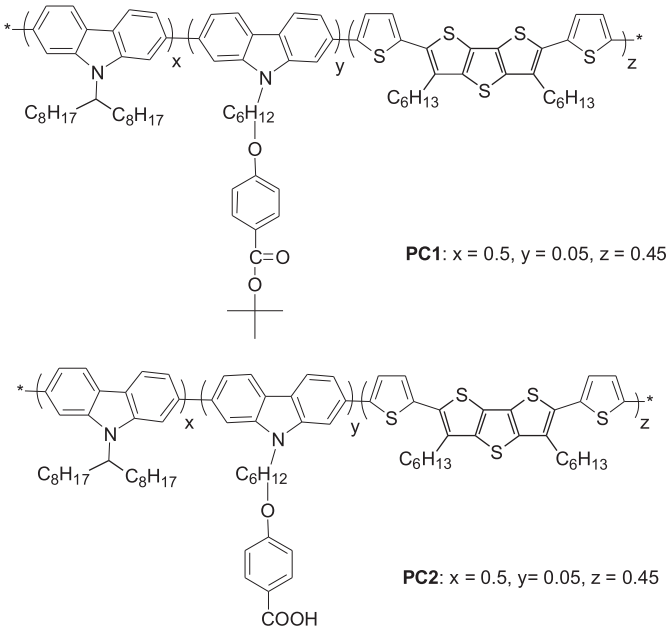

Fig. 1. Chemical structures of polymers **PC1** and **PC2**.

Dithieno[3,2-b:2′,3′-d]thiophene (DTT) is a sulfur rich (three-S atoms) and electron rich segment, and serves as an important building block of a wide variety of materials for electronic and optical applications, such as electroluminescence, two photon absorptions, nonlinear optics, photochromism, OFETs, and OPVs [14]. Besides, the fused aromatic rings can make the polymer backbones more rigid and coplanar, therefore enhancing effective π-conjugation lengths, lowering band gaps, and extending absorption lengths. Powder X-ray diffraction (XRD) analyses suggested that these copolymers formed self-assembled π–π stacking and pseudo-bilayered structures [15]. Molecules containing fused ring systems intend to maximize the π-orbital overlaps by restricting intramolecular rotation in these systems and possibly to induce face-to-face π–π stackings, facilitating intermolecular hoppings and charge transports [14]. In order to increase the solubility in poly(DTT) without causing any additional twisting of the repeating units in the resulting polymers, alkyl-substituted thiophene units were incorporated into the polymer backbones as copolymers to fabricate OPVs [16] and OFETs [17].

Based on this concept, two different moieties, i.e., fused dithienothiophene and carbazole, were utilized as donor monomers to synthesize fused dithienothiophene-based polymers **PC1**–**PC2** (see Fig. 1). In order to integrate electron donor polymers (**PC1**–**PC2**) with electron acceptors, pyridyl-surface-modified ZnO nanoparticles (**ZnOpy**) were synthesized according to Scheme 1. Compared with those reported fused dithienothiophene-based polymers, polymers **PC1**–**PC2** showed much improved open circuit voltage (V_{oc}) values with a highest open-circuit voltage of up to 0.88 V (in **PC2**) as well as suitable electronic energy levels and good processabilities for PSC applications. So far, the preliminary PSC performance of these structurally related copolymers showed the best PCE value of up to 0.55% while blended with **ZnOpy** and PCBM in a weight ratio of 1:0.05:1, with a short circuit current density (I_{sc}) of 2.11 mA/cm^2, an open circuit voltage (V_{oc}) of 0.88 V, and a fill factor (FF) of 0.29 under the solar simulator adjusted to give 100 mW/cm^2 of AM1.5 G irradiation. Although the results for the PCE values of these non-optimized PSCs are not sufficiently high enough, this research affords a new concept to incorporate electron donor polymers and electron acceptor surface-modified ZnO nanoparticles to the nanocomposite design.

2. Experimental

2.1. Materials

All chemicals and solvents were used as received. 2,7-dibromo-9-(heptadecan-9-yl)-9H-carbazole [9], 2,7-dibromo-carbazole [9], and 3,5-didecanyldithieno[3,2-b:2′3′-d]thiophene) [18,19] were synthesized according to the literature procedures. The detailed synthetic routes of polymers **PC1**–**PC2** will be published somewhere later. The synthetic routes of surface-modified ZnO nanoparticles (**ZnOpy**) are shown in Scheme 1. ZnO nanoparticles were synthesized by following the literature procedures [20]. Chemicals and solvents were reagent grades and purchased from Aldrich, ACROS, TCI, and Lancaster Chemical Co. Toluene, tetrahydrofuran, and diethyl ether were distilled to keep anhydrous before use.

2.2. Measurements and characterization

1H NMR spectra were recorded on a Varian Unity 300 MHz spectrometer using $CDCl_3$ solvents. Elemental analyses were performed on a HERAEUS CHN-OS RAPID elemental analyzer. Transition temperatures were determined by differential scanning calorimetry (DSC, Perkin-Elmer Pyris 7) with a heating and cooling rate of 10 °C/min. Thermogravimetric analyses (TGA) were conducted with a TA instrument Q500 at a heating rate of 10 °C/min under nitrogen. Gel permeation chromatography (GPC) analyses were conducted on a Waters 1515 separation module using polystyrene as a standard and THF as an eluent. UV–visible absorption and photoluminescence (PL) spectra were recorded in dilute chlorobenzene solutions (10^{-6} M) on a HP G1103A and Hitachi F-4500 spectrophotometer, respectively. Solid films of UV–vis and PL measurements were spin-coated on quartz

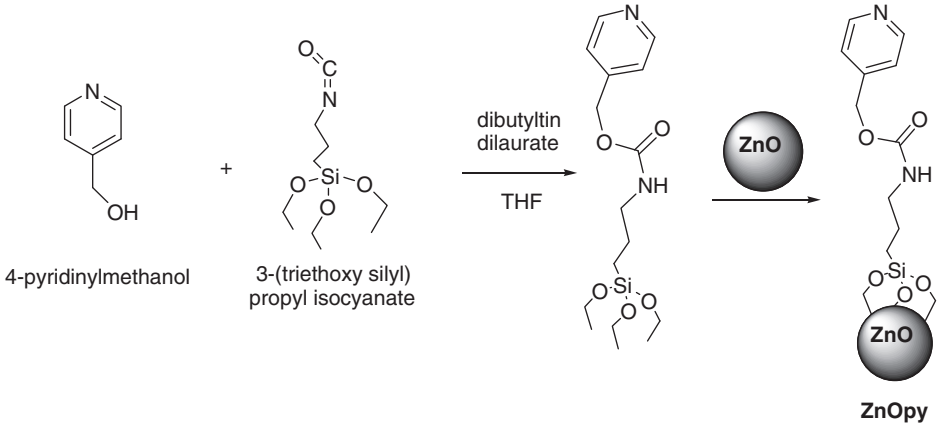

Scheme 1. Synthetic routes of surface-modified ZnO (**ZnOpy**).

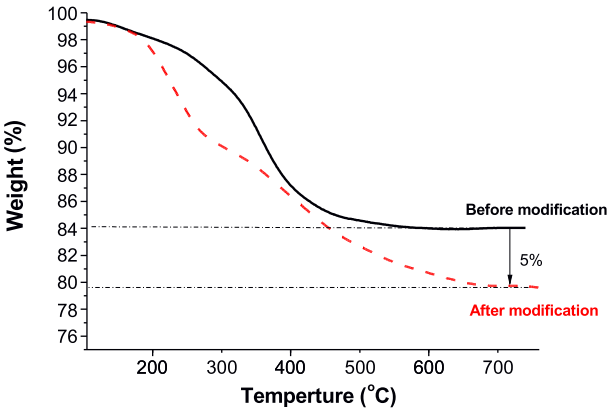

Fig. 2. Thermogravimetric curves of ZnO nanoparticles before and after pyridyl-surface-modification.

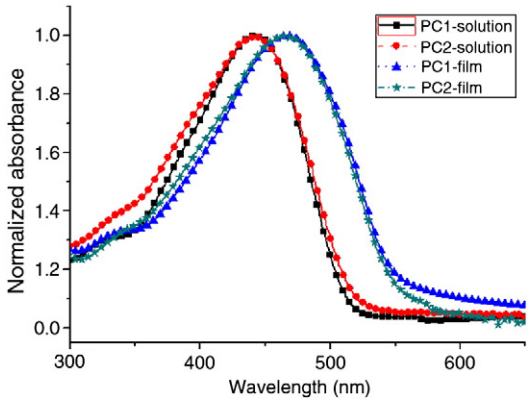

Fig. 3. Normalized optical absorption spectra of polymers **PC1–PC2** in solutions (chlorobenzene) (10^{-6} M), and solid films (spin-coating from chlorobenzene solutions).

substrates from chlorobenzene solutions with a concentration of 10 mg/mL. Cyclic voltammetry (CV) measurements were performed using a BAS 100 electrochemical analyzer with a standard three-electrode electrochemical cell in a 0.1 M tetrabutylammonium hexafluorophosphate ($TBAPF_6$) solution (in chorobenzene) at room temperature with a scanning rate of 50 mV/s. In each case, a carbon working electrode coated with a thin layer of these copolymers, a platinum wire as the counter electrode, and a silver wire as the quasi-reference electrode were used. Ag/AgCl (3 M KCl) electrode was served as a reference electrode for all potentials quoted herein. During the CV measurements, the solutions were purged with nitrogen for 30 s, and the redox couple ferrocene/ferrocenium ion (Fc/Fc^+) was used as an external standard. The corresponding HOMO and LUMO levels in copolymer films of **PC1**–**PC2** and **ZnOpy** were calculated from $E_{ox/onset}$ and $E_{red/onset}$ values of the electrochemical experiments. The LUMO value of PCBM [19] was in accordance with the literature data. Each onset potential in the CV measurements was defined by the intersection of two tangents drawn at the rising current and background current. Film thickness and morphology were determined using a Veeco Nanoscope DI 3100 AFM microscope operating in the tapping mode. The actual z resolution of AFM measurements is 50 nm.

2.3. Device fabrication and characterization of polymer solar cells

The photovoltaic cell (PVC) device structure used in this study was a sandwich configuration of ITO/PEDOT:PSS/active layer/Ca/Al, where the active layer was made of electron donor polymers **PC1**–**PC2** mixed with both electron acceptors **ZnOpy** and [6,6]-phenyl C_{61} butyric acid methyl ester (PCBM) in the weight ratios of polymer:**ZnOpy**:PCBM = 1:0.05:1 and 1:0.1:1. The PVC devices were fabricated according to the procedures similar to those of EL devices. The ITO coated glass substrates were pre-cleaned and treated with oxygen plasma prior to use. A thin layer (~50 nm) of PEDOT:PSS was spin-coated on an ITO substrate and heated at 130 °C for 1 h. Subsequently, the preliminary active layer was prepared by spin coating from composite solutions of **PC1**–**PC2**:**ZnOpy**:PCBM in chlorobenzene (10 mg/mL) on the top of PEDOT:PSS layer. The spin rate was about 800 rpm, and the thickness of the active layer was typically ranged at 100–160 nm, unless the detailed thickness is specified. The PVC devices were completed by deposition with 1 nm of Ca and 120 nm of Al. The film thicknesses were measured by a profilometer (Dektak3, Veeco/Sloan Instruments Inc., USA). For photovoltaic measurements, *I–V* curves were recorded under a solar simulator with AM 1.5 irradiation (at 100 mW/cm^2). A 300 W xenon lamp (Oriel, #6258) with AM 1.5 filter (Oriel, #81080 kit) was used as the white light source, and the optical power shone on the sample was 100 mW/cm^2 detected by Oriel thermopile 71964. The *I–V* characteristics were measured using a CHI 650B potentiostat/galvanostat. The external quantum efficiency (EQE) was measured using a CHI 650B coupled with Oriel Cornerstone 260 monochromator. All PVC devices were prepared and measured under ambient conditions.

2.4. Synthesis

The synthetic routes of surfactant and pyridyl-modified ZnO (**ZnOpy**) are shown in Scheme 1.

2.5. (Pyridine-4-yl) methyl-3-(trethoxysily)propylcarbamate

4-Pyridinylmethanol (628 mg, 5.76 mmol) and 3-(triethoxysilyl) propyl isocyanate (2.8 g, 11.48 mmol) were dissolved in dry THF (40 mL) and stirred in a flask. Besides, dibutyltin dilaurate (36 mg, 0.058 mmol) was added dropwise. The mixture was refluxed overnight. Solvent was removed under vacuum, and the crude product was purified by flash column chromatography using hexane/ethyl acetate = 1:2, v/v as eluent. Subsequently, the pure compound was obtained as a yellow powder. Yield: 1.84 g (66%). 1H NMR (300 MHz, $CDCl_3$): δ (ppm) 8.68 (dd, 2H), 8.05 (d, 1H), 7.52 (dd, 2H), 5.34 (s, 2H), 3.82 (quart, 6H), 3.18 (m, 2H), 1.87 (quint, 2H), 1.22 (t, 9H), and 0.63 (t, 2H). HRMS (EI): calculation For C16H28N2O5Si, 356.49; found 356. Element analysis calculation for C16H28N2O5Si: N, 7.86; C, 53.91; and H, 7.92. Found: N, 7.90; C, 53.94; and H, 7.81.

Table 1
Molecular weights, yields, and thermal data of polymers **PC1**–**PC2**.

Polymer	M_n[a]	M_w[b]	PDI[c]	Tg[d] (°C)	T_d[e] (°C)	Yield (%)
PC1	19200	53100	2.7	135	366	79.5
PC2	18200	50100	2.7	143	408	80.0

[a] Number average molecular weight.
[b] Weight average molecular weight.
[c] Polydispersity indices (PDI = Mw/Mn).
[d] Glass transition temperature.
[e] Decomposition temperature at 5% weight loss.

Table 2
Photophysical data of polymers **PC1–PC2** in chloroform solutions and solid films.

Polymer	$\lambda_{abs,sol}$[a] (nm)	$\lambda_{abs,film}$[b] (nm)	$\lambda_{PL,film}$[b] (nm)
PC1	442	465	543
PC2	441	465	–

[a] The absorption spectra were recorded in dilute chlorobenzene solution at room temperature.
[b] The absorption and PL films were spin-coated from 10 mg/1 mL chlorobenzene solution.

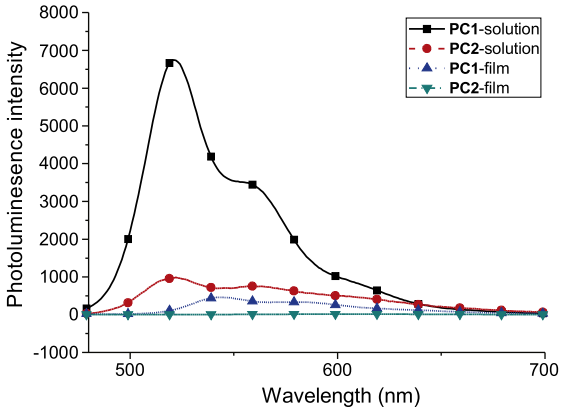

Fig. 4. Normalized photoluminescence (PL) spectra of polymers **PC1–PC2** in solutions (chlorobenzene) (10^{-6} M), and solid films (spin-coating from chlorobenzene solutions).

2.6. Synthesis of pyridyl-modified ZnO nanoparticles (ZnOpy)

ZnO nanoparticles [20] were dissolved and stirred in dry toluene (10 mL). Then, (pyridine-4-yl) methyl-3-(trethoxysily)propylcarbamate (1 g, 0.058 mmol) was added dropwise. The mixture was stirred to react overnight at 100 °C. The resulting precipitates were isolated by centrifugation along with decantation, and then were rewashed several times to remove all residues. The resulting product was subsequently collected and dried under vacuum. The amount of pyridyl surface-modifiers attached to ZnO nanoparticle surface can be estimated by TGA analysis and was found ca. 5 wt.% in Fig. 2. In addition, the sizes of ZnO nanoparticles surface-modified with pyridyl surfactants (**ZnOpy**) were ca. 3–4 nm.

3. Results and discussion

3.1. Thermal properties

The thermal stabilities and phase transition properties of polymers **PC1–PC2** were characterized by thermogravimetric analyses (TGA) and differential scanning calorimetry (DSC) measurements under nitrogen atmosphere, and the thermal decomposition temperatures (T_d) and melting points (T_m) are summarized in Table 1. It is apparent that all copolymers exhibited good thermal stabilities, which showed less than 5% weight loss upon heating to 366–408 °C. Regarding DSC experiments, samples (weighted 1–5 mg) sealed in an aluminum pan were operated at 30–250 °C under N_2 atmosphere with a scan rate of 10 °C/min. These polymers showed relatively sharp transitions appearing around 135–143 °C, which were attributed to the melting

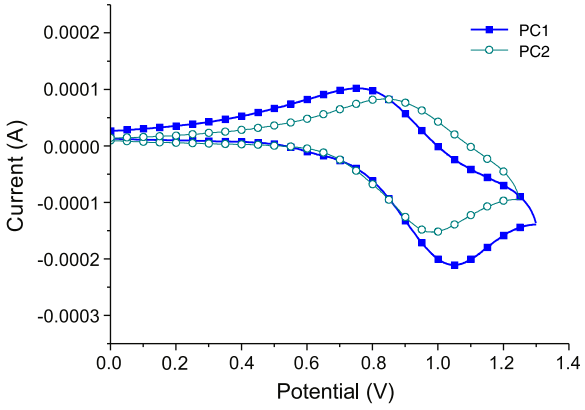

Fig. 5. Cyclic voltammograms of polymers **PC1–PC2** (solid films) at a scan rate of 100 mV/s.

Table 3
Electrochemical potentials, energy levels, and band gap energies of polymers **PC1–PC2**[a].

Polymer	$\lambda_{onset,abs}$ (nm)	E_g[a] (eV)	$E_{1/2}$[b] (eV)	HOMO[c] (V)	LUMO[d] (V)
PC1	550	2.25	0.91	−5.60	−3.35
PC2	551	2.25	0.91	−5.60	−3.35

[a] The optical band gap was obtained from the equation $E_g^{opt} = 1240/\lambda_{onset}$.
[b] $E_{1/2}$ was the average value of oxidation and reduction potential.
[c] $E_{HOMO} = [-(E_{1/2} - 0.11) - 4.8]$ eV where 0.11 V is the value for ferrocene vs Ag/Ag+ and 4.8 eV is the energy level of ferrocene below the vacuum.
[d] LUMO = HOMO − E_g.

of the polymer backbones, and two polymers exhibited the glass transition (Tg) temperatures at 135 °C and 143 °C for **PC1** and **PC2**, respectively. The Tg and T_d values of **PC2** are higher than that of **PC1**, implying that the polymer networks formed by H-bonds (due to acid groups) of **PC2** make the structure more rigid.

3.2. Optical properties

The optical absorption spectra of polymers **PC1–PC2** in chlorobenzene solutions (10^{-6} M) and solid films are shown in Fig. 3, and their photophysical properties are demonstrated in Table 2. As can be seen, the absorption spectra of polymers **PC1–PC2** covered broad wavelength ranges for both solutions and solid films. Similar maximum absorption wavelengths (442 and 441 nm) of **PC1** and **PC2** in chlorobenzene solutions were observed. These donor polymers (**PC1–PC2**) achieved the absorption spectra in the visible range of 350–580 nm (with tailing up to around 650 nm) in solid films. Due to the π–π stacking of these polymer chains in solids, both maximum absorption wavelengths in solid films were red-shifted to ca. 465 nm in polymers **PC1** and **PC2**. In addition, the long tailing around 650 nm in the absorption spectra of **PC1–PC2** in both solutions and solid films were observed. As shown in Table 2, the optical band gaps ($E_{g,opt}$) of 2.25 eV in polymers **PC1–PC2** can be determined by the cut off of the absorption spectra in solid films.

The photoluminescence (PL) spectra of polymers **PC1** and **PC2** in chlorobenzene solutions and solid films excited at incident wavelengths of 465 nm are shown in Fig. 4, respectively. The PL emission spectra of the polymers in solutions were dramatically quenched. Interestingly, in contrast to polymer **PC1** in Fig. 4, the PL spectra of **PC2** containing acid moieties were completely quenched in solid films. The corresponding optical properties of these copolymers in solid films, including the broad and strong optical absorptions, proposed their potential applications in the photovoltaic cells described below.

3.3. Electrochemical characterization

The electronic states, i.e. highest occupied molecular orbital (HOMO) and lowest unoccupied molecular orbital (LUMO) levels, of the polymers were investigated by cyclic voltammetry (CV) in order to understand the charge injection processes in these polymers and their PSC devices. The oxidation and reduction cyclic voltammograms of polymers **PC1–PC2** in solid films are displayed in Fig. 5. In order to obtain the solid films with an equal thickness, the concentrations in the THF solutions and film forming conditions were kept constant (ca. 5 mg/mL). The electrochemical measurements of the formal potentials, onset potentials, and band gaps, along with the estimated positions of the upper edges of the valence band (HOMO levels) and the lower edges of the conduction band (LUMO levels) are summarized in Table 3. On the contrary, all polymers **PC1–PC2** exhibited one quasi-reversible oxidation peaks as evident from the areas and close proximity of the anodic and cathodic scans in Fig. 5, which are a good sign for high structural stability in the charged state. As illustrated in Table 3, the formal oxidation potentials of these polymers were in the range of 0.7–1.1 V.

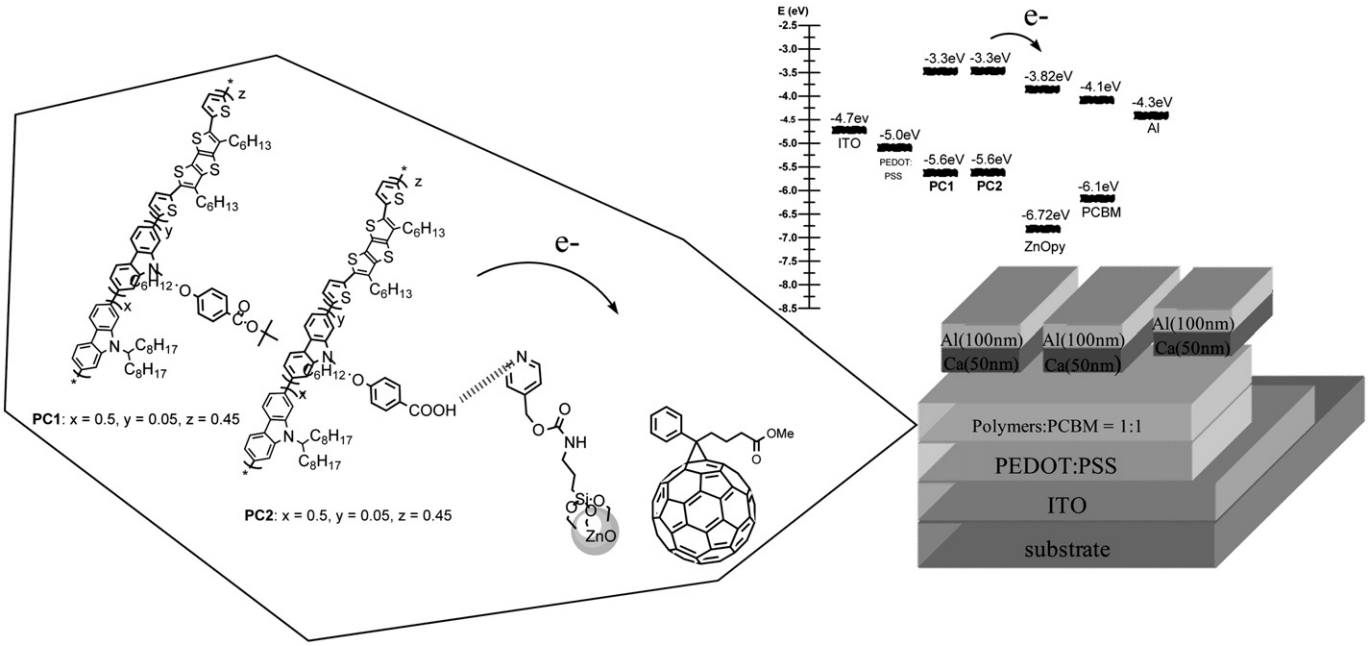

Fig. 6. Energy band diagram of HOMO/LUMO levels for electron donor polymers **PC1**–**PC2**, electron acceptors **ZnOpy** and PCBM, and the work functions of ITO and Al.

The moderate onset oxidation potentials of polymers **PC1–PC2** occurred between 0.7 and 1.1 V from which the estimated HOMO levels of −5.60 eV and LUMO levels of ca. −3.35 eV were acquired according to the following equation: [22,23] $E_{HOMO/LUMO} = [-(E_{onset\ (vs\ Ag/AgCl)} - E_{onset\ (Fc/Fc+\ vs\ Ag/AgCl)}) - 4.8]$ eV, where 4.8 eV is the energy level of ferrocene below the vacuum level and $E_{onset\ (Fc/Fc+\ vs\ Ag/AgCl)} = 0.4$ eV. In contrast, the electrochemical reductions of polymers **PC1–PC2** showed similar LUMO energy levels at ca. −3.35 eV, which represent to possess high electron affinities and also make these polymers suitable electron donors for electron injection and transporting to **ZnOpy** and PCBM acceptors (with 0.4 eV offsets in LUMO levels regarding PCBM with a LUMO level of −3.75 eV [20], as shown in Fig. 6

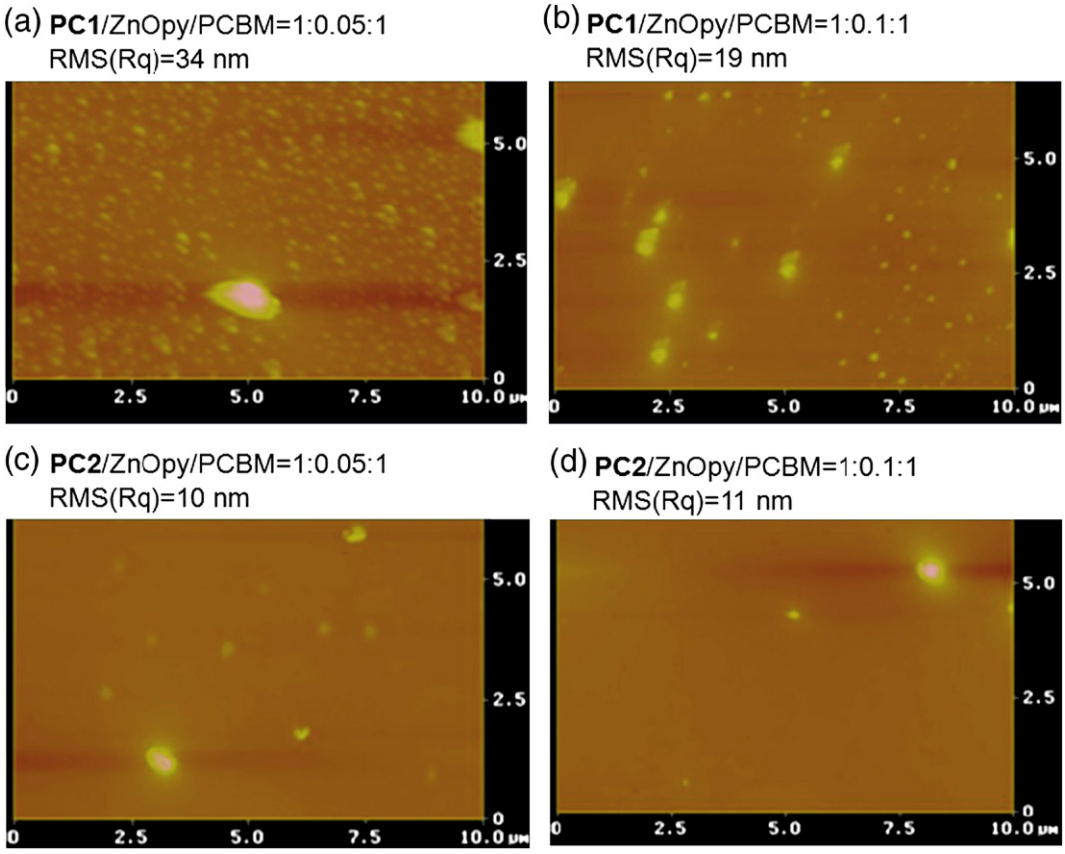

Fig. 7. The AFM images obtained for films of **PC1**/**ZnOpy**/PCBM and **PC2**/**ZnOpy**/PCBM containing different amounts of nanoparticles and fullerene.

Table 4
Photovoltaic properties of PSC devices containing an active layer of Polymer:**ZnOpy**:PCBM (w/w) with a device configuration of ITO/PEDOT:PSS/Polymer:**ZnOpy**:PCBM/Ca/Al[a].

Active layer (polymer:**ZnOpy**:PCBM)	V_{oc} (V)	J_{sc} (mA/cm2)	FF (%)	PCE (%)
PC1:**ZnOpy**:PCBM = 1:0.05:1	1.79	0.79	0.31	0.44
PC1:**ZnOpy**:PCBM = 1:0.1:1	1.57	0.77	0.29	0.35
PC2:**ZnOpy**:PCBM = 1:0.05:1	2.11	0.88	0.29	0.55
PC2:**ZnOpy**:PCBM = 1:0.1:1	2.14	0.82	0.29	0.51

[a] Measured under AM 1.5 irradiation, 100 mW/cm^2.

for the polymeric bulk heterojunction solar cell devices [21]. Interestingly, the energy band gaps $E_{g,ec}$ measured directly from CV ($E_{g,ec} = E_{ox/onset} - E_{red/onset}$, where $E_{g,ec}$ values are 2.25 eV) are close to the optical band gaps ($E_{g,opt}$ are 2.25 eV) acquired from the absorption spectra.

3.4. Morphology

The AFM topographies by the tapping mode of polymer blends (**PC1–PC2**:**ZnOpy**:PCBM = 1:0.05:1 and 1:0.1:1 in wt. ratios) were investigated via casting films of dichlorobenzene solutions as shown in Fig. 7, where the bumps on the surface views are possibly attributed to the aggregation of ZnO nanoparticles (**ZnOpy**) and polymers (**PC1–PC2**). The results show that the morphologies of blends **PC1**/**ZnOpy**/PCBM have larger roughnesses (34 and 19 nm in Fig. 7(a) and (b), respectively) than those (10 and 11 nm in Fig. 7(c) and (d), respectively) of blends **PC2**/**ZnOpy**/PCBM. **PC1**/**ZnOpy**/PCBM films exhibited larger roughness variations than **PC2**/**ZnOpy**/PCBM. The roughness and phase separation must be controlled/optimized in order to improve the efficiency of devices [24–26]. It is worthy to mention that the solid films of blended **PC1**:**ZnOpy**:PCBM in different ratios of 1:0.05:1 and 1:0.1:1 w/w showed rougher surfaces, but the larger values of rms roughnesses (34 and 19 nm, respectively) were contributed from the aggregation of nanoparticles due to no interaction between polymer and nanoparticles, which reduced the interfaces between donor (polymers) and acceptor (**ZnOpy**:PCBM) significantly. Owing to the unfavorable morphologies for charge transport offered by the aggregation of nanoparticles, the PSC devices based on **PC1** gave relatively low current densities (*I*sc) as shown in Table 4.

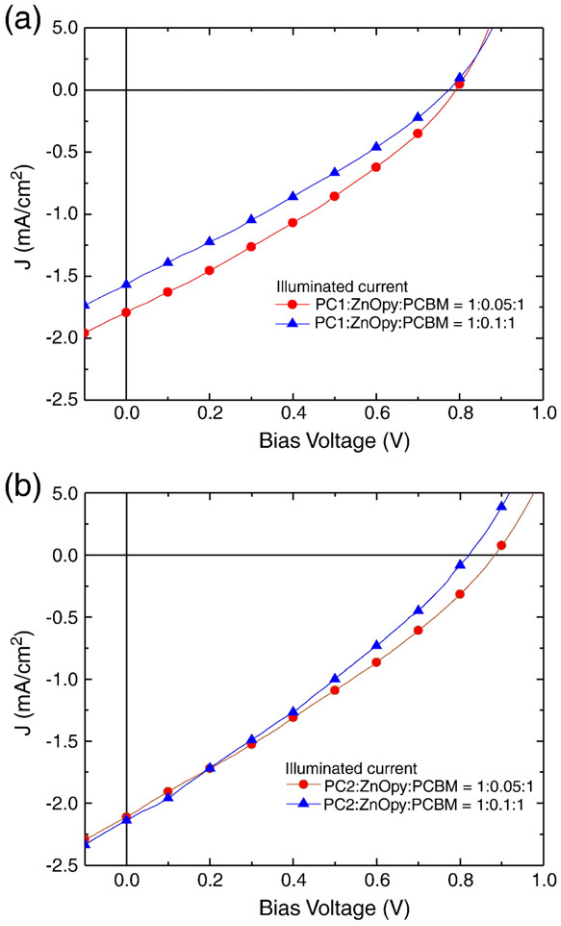

Fig. 8. *I–V* curves of solar cells under simulated AM 1.5 solar irradiation with an active layer of (a) **PC1**:**ZnOpy**:PCBM (with different weight ratios of **ZnOpy**) and (b) **PC2**:**ZnOpy**:PCBM (with different weight ratios of **ZnOpy**).

3.5. Polymeric photovoltaic cell properties

The motivation for the design and syntheses of the conjugated polymers is to look for new polymers for the application of PSCs. To investigate the potential use of polymers **PC1–PC2** in PSCs, bulk heterojunction devices were fabricated from an active layer in which polymers **PC1–PC2** were blended with the **ZnOpy** and PCBM. The PSC devices with a configuration of ITO/PEDOT:PSS/**PC1-PC2**:**ZnOpy**:PCBM(w/w)/Ca/Al were fabricated by depositing a thin layer (ca. 50 nm) of PEDOT:PSS onto patterned ITO slides. The active layer (ca. 100–160 nm) consisting of **PC1–PC2**, **ZnOpy** and PCBM (w/w) was then deposited from a solution (10 mg/mL in dichlorobenzene) by a spin rate of 500 rpm on the PEDOT:PSS film, and followed by the deposition of Ca (ca. 50 nm) and aluminum (100 nm) back electrodes. The PSC devices were measured under AM 1.5 illuminations for a calibrated solar simulator with an intensity of 100 mW/cm^2. The preliminarily obtained properties are summarized in Table 4, and the typical *I–V* characteristics of all PSC devices are shown in Fig. 8. The PSC device containing polymer **PC2** blended with **ZnOpy** and PCBM acceptors had the highest PCE value of 0.55% with the values of $I_{sc} = 2.11$ mA/cm^2, FF = 29.4%, and $V_{oc} = 0.88$ V.

4. Conclusions

The concept of supermolecular interactions, such as H-bonds formed between conjugated polymers (**PC1–PC2**) and surface-modified nanoparticles ZnO (**ZnOpy**), has been introduced by the syntheses of **ZnOpy** nanoparticles and two fused dithienothiophene/carbazole-based polymers. The band gaps and the HOMO/LUMO energy levels of these resulting copolymers can be finely tuned as demonstrated by the investigation of optical absorption properties and electrochemical studies. The pyridyl surfactants of **ZnOpy** nanoparticles (as electron acceptors to partially replace expensive electron acceptor PCBM) not only induce supramolecular interactions with benzoic acid pendants of polymer **PC2** via H-bonds, but also enhance the homogeneous dispersions of **ZnOpy** nanoparticles in polymer **PC2**. Thus, the PSC device containing ternary components of polymer **PC2** blended with **ZnOpy** and PCBM acceptors (**PC2**:**ZnOpy**:PCBM = 1:0.05:1) had the power conversion efficiency of up to 0.55%, which gave the best performance with the values of $I_{sc} = 2.11$ mA/cm^2, FF = 29.4%, and $V_{oc} = 0.88$ V.

Acknowledgements

The financial supports of this project provided by the National Science Council of Taiwan (ROC) through NSC 97-2113-M-009-006-MY2 and National Chiao Tung University through 97W807 are acknowledged.

References

[1] G. Yu, J. Gao, J.C. Hummelen, F. Wudl, A.J. Heeger, Science 270 (1995) 1789.
[2] B.C. Thompson, J.M.J. Fréchet, Angew. Chem. Int. Ed. 47 (2008) 58.

[3] T. Kietzke, R.Y.C. Shin, D. Ayuk Mbi Egbe, Z.K. Chen, A. Sellinger, Macromolecules 40 (2007) 4424.
[4] C. Uhrich, R. Schueppel, A. Petrich, M. Pfeiffer, K. Leo, E. Brier, P. Kilickiran, P. Baeuerle, Adv. Funct. Mater. 17 (2007) 2991.
[5] D.J.D. Moet, L.J.A. Koster, B. de Boer, P.W.M. Blom, Chem. Mater. 19 (2007) 5856.
[6] W.J.E. Beek, M.M. Wienk, R.A.J. Janssen, Adv. Mater. 16 (2004) 1009.
[7] L.J.A. Koster, W.J.V. Strien, W.J.E. Beek, P.W.M. Blom, Adv. Funct. Mater. 17 (2007) 1297.
[8] J.N.D. Freitas, I.R. Grova, L.C. Akcelrud, E. Arici, N.S. Sariciftcic, A.F. Nogueira, J. Mater. Chem. 20 (2010) 4845.
[9] N. Blouin, A. Michaud, M. Leclerc, Adv. Mater. 19 (2007) 2295.
[10] J. Li, F. Dierschke, J. Wu, A.C. Grimsdale, K. Müllen, J. Mater. Chem. 16 (2006) 96.
[11] J.F. Morin, M. Leclerc, D. Adès, A. Siove, Macromol. Rapid Commun. 26 (2005) 761.
[12] N. Drolet, J.F. Morin, N. Leclerc, S. Wakim, Y. Tao, M. Leclerc, Adv. Funct. Mater. 15 (2005) 1671.
[13] N. Leclerc, A. Michaud, K. Sirois, J.F. Morin, M. Leclerc, Adv. Funct. Mater. 16 (2006) 1694.
[14] Z. Shiming, F. Haijun, L. Yao, Z. Guangjin, L. Qikai, L. Yongfang, Z. Xiaowei, J. Polym. Sci. Part A: Polym. Chem. 47 (2009) 2843.
[15] K.C. Li, J.H. Huang, Y.C. Hsu, P.J. Huang, C.W. Chu, J.T. Lin, K.C. Ho, K.H. Wei, H.C. Lin, Macromolecules 42 (2009) 3681.
[16] A.J. Moulé, A. Tsami, T.W. Bünnagel, M. Forster, N.M. Kronenberg, M. Scharber, M. Koppe, M. Morana, C.J. Brabec, K. Meerholz, U. Scherf, Chem. Mater. 20 (2008) 4045.
[17] J. Li, F. Qin, C.M. Li, Q.L. Bao, M.B. Chan-Park, W. Zhang, J.G. Qin, B.S. Ong, Chem. Mater. 20 (2008) 2057.
[18] M. He, F. Zhang, J. Org. Chem. 72 (2007) 442.
[19] G. Dennler, M.C. Scharber, C.J. Brabec, Adv. Mater. 21 (2009) 1323.
[20] C.H. Hung, W.T. Whang, J. Mater. Chem. 15 (2005) 267.
[21] V.D. Mihailetchi, J.K.J.v. Duren, P.W.M. Blom, J.C. Hummelen, R.A.J. Janssen, J.M. Kroon, M.T. Rispens, W.J.H. Verhees, M.M. Wienk, Adv. Funct. Mater. 13 (2003) 43.
[22] C.J. Brabec, N.S. Sariciftci, J.C. Hummelen, Adv. Funct. Mater. 11 (2001) 15.
[23] M. Shahid, R.S. Ashraf, E. Klemm, S. Sensfuss, Macromolecules 39 (2006) 7844.
[24] H. Hoppe, M. Niggemann, C. Winder, J. Kraut, R. Hiesgen, A. Hinsch, D. Meissner, N.S. Sariciftci, Adv. Funct. Mater. 14 (2004) 1005.
[25] X. Yang, J. Loos, S.C. Veenstra, W.J.H. Verhees, M.M. Wienk, J.M. Kroon, M.A.J. Michels, R.A.J. Janssen, Nano Lett. 5 (2005) 579.
[26] H. Hoppe, N.S. Sariciftci, J. Mater. Chem. 16 (2006) 45.